Genetic structure of prey populations underlies the geographic mosaic of arms race coevolution

Authors: Michael T.J. Hague[1*], Amber N. Stokes[2], Chris R. Feldman[3], Edmund D. Brodie, Jr.[4], Edmund D. Brodie III[5]

Affiliations:

[1] Department of Biological Sciences, University of Montana, Missoula, MT, USA.

[2] Department of Biology, California State University, Bakersfield, CA, USA.

[3] Department of Biology, University of Nevada, Reno, NV, USA.

[4] Department of Biology, Utah State University, Logan, UT, USA.

[5] Department of Biology, University of Virginia, Charlottesville, VA, USA.

[*] Correspondence to:

Michael T.J. Hague

Department of Biological Sciences, University of Montana

32 Campus Dr. HS 104, Missoula, MT 59812, USA

Tel: (406) 243-2182

Email: michael.hague@mso.umt.edu

Abstract:

Reciprocal adaptation is the hallmark of arms race coevolution[1,2], but the symmetry of evolutionary change in each species is often untested even in the best-studied battles between natural enemies[3]. We tested whether prey and predator exhibit symmetrical evidence of local co-adaptation in the classic example of a geographic mosaic of coevolution between toxic newts (*Taricha granulosa*) and resistant garter snakes (*Thamnophis sirtalis*)[4,5]. Levels of newt toxin and snake resistance are functionally matched in populations across the landscape, implying that mosaic variation in the armaments of both species results from the local pressures of reciprocal selection. Contrary to conventional wisdom, however, we found that landscape-wide variation in the newt toxin is best predicted by neutral population divergence rather than the resistance of local predators. On the other hand, snake resistance is clearly explained by prey toxin levels. Prey populations seem to structure variation in defensive toxin levels across the geographic mosaic, which in turn determines selection on predator resistance. Exaggerated armaments suggest coevolution occurs in certain hotspots, but our results imply that neutral processes including gene flow—rather than reciprocal adaptation—comprise the greatest source of variation across the coevolutionary mosaic.

Main Text:

Coevolutionary dynamics result from the reciprocal selection generated between interacting species[2,6]. Adaptation and counter-adaptation occur at the phenotypic interface of coevolution, the traits in each species that mediate interactions[1,7]. Because species interactions and their fitness consequences vary spatially, heterogeneity in the form of reciprocal selection is expected to generate a geographic mosaic of coevolution in which phenotypes of both species covary due to local conditions[6,8–10]. Coevolving species often exhibit matched trait variation across the landscape, for example, in seed traits and their predators[8,10] or host and pathogen genotypes[11,12], a pattern typically interpreted as a signature of local co-adaptation.

However, a geographic mosaic of matched phenotypes may not be solely the result of reciprocal co-adaptation[3,5]. A simpler, non-adaptive explanation for matched trait variation involves the spatial population structure and ancestry of each species. Common barriers to dispersal or a shared biogeographic history, for example, could structure phenotypic divergence congruently in co-occurring species[13]. Only when phenotypic variation deviates from the neutral expectations of population structure in both species can we infer local adaptation in the geographic mosaic of coevolution[3]. Otherwise, drift, gene flow, and phylogeography provide a parsimonious explanation for patterns of divergence across the landscape.

In western North America, rough-skinned newts (*Taricha granulosa*) secrete the deadly neurotoxin tetrodotoxin (TTX), which binds to the outer pore of voltage-gated sodium channels (Na_V) and prevents the initiation of action potentials[14,15]. Common garter snakes (*Thamnophis sirtalis*) exhibit resistance to TTX that is largely due to specific amino acid substitutions in the fourth domain pore-loop (DIV p-loop) of the skeletal muscle sodium channel ($Na_V1.4$) that disrupt toxin-binding (Fig. 1)[16,17]. Channel-level TTX resistance conferred by each allele in the

63 DIV p-loop is tightly correlated with muscle and whole-animal levels of phenotypic resistance in
64 *Th. sirtalis*[16–18]. TTX-resistant alleles occur at high frequency in coevolutionary "hotspots" with
65 highly toxic newts, but are largely absent in surrounding "coldspots" where newts are non-
66 toxic[19]. Quantitative levels of newt toxin and snake resistance are functionally matched in many
67 co-occurring populations[4,5], implying a geographic mosaic of coevolution that is largely the
68 result of co-adaptation to local pressures in the arms race. Consequently, population divergence
69 in both prey toxin and predator resistance is presumed to represent adaptive deviations from the
70 selectively neutral expectations of population structure and ancestry.

71 We tested whether neutral processes could account for localized trait-matching in this
72 textbook example of a geographic mosaic of coevolution. We conducted fine-scale population
73 sampling of newts (n=138) and garter snakes (n=169) along a latitudinal transect of nine
74 locations on the Pacific Coast in Washington and Oregon (USA) that spans the geographic
75 mosaic (Fig. 1, Supplementary Table S1), ranging from low levels of newt toxin and snake
76 resistance (northern Washington) to a hotspot of extreme escalation in both species (central
77 Oregon). At each location, we characterized levels of TTX in newt populations and TTX
78 resistance in garter snakes, including whole-animal phenotypic resistance and $Na_V1.4$ channel
79 genotypes. We then compared these data to neutral patterns of population genomic variation in
80 each species using single nucleotide polymorphisms (SNPs) in each species.

81 Spatial patterns of newt TTX and snake resistance were broadly consistent with previous
82 work indicating arms race coevolution has led to the closely matched phenotypes in each
83 species[5]. The degree of functional overlap in quantitative levels of prey toxin and predator
84 resistance suggest that locally varying reciprocal selection occurs throughout the transect
85 (Extended Fig. 1)[5]. TTX levels ($\mu g/cm^2$) of newts varied by population (ANOVA;

86 F[8,114]=37.43, p<0.001) and by sex (F[1,114]=4.37, p=0.039) along the latitudinal transect
87 (Fig. 1; Supplementary Table S1). TTX resistance (50% MAMU dose) of snakes also varied by
88 population (according to non-overlapping 95% confidence intervals; Fig. 1; Supplementary
89 Table S1) and was closely correlated with prey toxin (regression of distance matrices, p=0.021;
90 Table 1). The presence of TTX-resistant alleles in the $Na_V1.4$ channel co-varied with phenotypic
91 resistance in garter snakes, such that pairwise F_{ST} divergence at the DIV p-loop was correlated
92 with population divergence in phenotypic resistance (Mantel test, r=0.47, p=0.032).
93 Variation in levels of newt TTX, however, was best predicted by neutral population
94 divergence, suggesting that reciprocal co-adaptation cannot fully explain the geographic mosaic
95 of matched prey toxin and predator resistance. We used neutral SNPs to assess population
96 genetic structure in prey and predator and found a pattern of isolation-by-distance (IBD) in both
97 species (distance-based redundancy analysis; newts, F=-38.528, p=0.002; snakes, F=22.021,
98 p=0.001). Principal coordinate (PCoA) and Bayesian clustering (STRUCTURE) analyses
99 indicated that newts and snakes each have a distinct spatial pattern of population structure along
100 the transect (Fig. 2, Extended Fig. 2). We generated distance matrices to test whether phenotypic
101 divergence in one species (e.g., newt TTX levels) is best explained by (1) neutral genomic
102 divergence (pairwise F_{ST}; Supplementary Table S4) or (2) phenotypic divergence in the natural
103 enemy (snake resistance). In univariate regressions, population divergence in the TTX level of
104 newts was strongly predicted by neutral F_{ST} divergence (R^2=0.414), as well as TTX resistance of
105 garter snakes (R^2=0.274; Table 1). F_{ST} divergence remained significant in the multiple
106 regression, indicating that population structure of newts predicts TTX levels, even after
107 controlling for TTX resistance of the predator (which was at best marginally significant;
108 p=0.065). In contrast, garter snake resistance was strictly predicted by newt toxin and not neutral

109 F_{ST} divergence. Both phenotypic resistance and F_{ST} divergence at the DIV p-loop (the site of
110 toxin-binding in $Na_V1.4$) were uncorrelated with neutral F_{ST} values in garter snakes (Table 1).
111 These results indicate that neutral genetic divergence is a key determinant of population
112 differences in prey toxin levels, which in turn predicts differences in TTX resistance among
113 predator populations. The geographic structure of newt populations appears to be so influential to
114 spatial dynamics that divergence in garter snake phenotypic resistance and F_{ST} at the DIV p-loop
115 are both significantly predicted by neutral F_{ST} divergence of newts (Table 1).
116 Clinal variation in TTX levels of newts is highly congruent with neutral genomic
117 variation based on the PCoA (Fig. 3) and Bayesian clustering analyses (Extended Fig. 3). TTX
118 resistance of garter snakes, in contrast, clearly deviates from neutral expectations to track
119 variation in prey toxin. Cline-fitting analyses show that prey toxin levels and predator resistance
120 are tightly matched along the 611 km transect; the geographic center points of each cline are
121 located just 64 km apart and do not differ statistically. The cline center of TTX-resistant alleles
122 in snakes is also located nearby, although it differed statistically from the center of newt TTX.
123 Despite similar phenotypic clines for both species, variation in levels of newt toxin showed an
124 even tighter match to clinal variation in neutral population structure. The center points of the
125 TTX and neutral clines were located only 19 km apart. PC 1 from the PCoA was a strong
126 predictor of variation in TTX levels (linear model; t-value=5.682, $p<0.001$), even after
127 controlling for the effect of TTX resistance of garter snakes (Supplementary Table S6).
128 Conversely, variation in phenotypic resistance and TTX-resistant alleles in snakes both deviated
129 significantly from the neutral cline (Fig. 3), such that resistance was not predicted by PCs 1 or 2
130 from the PCoA (Supplementary Table S6). The center points of the snake phenotypic resistance
131 and neutral clines were located a distant 310 km apart.

132 Levels of prey toxin and predator resistance are tightly matched across the landscape, but
133 this pattern does not appear to primarily result from local arms race co-adaptation. Although
134 predator resistance is geographically structured by a signature of local adaptation to prey, levels
135 of the prey toxin are structured in tight accordance with neutral population divergence. These
136 results imply that landscape-wide variation in newt toxin across the geographic mosaic is best
137 explained by non-adaptive processes, such as drift and historical biogeography, rather than local
138 variation in selection from predators. For example, latitudinal patterns of newt TTX and neutral
139 divergence are both consistent with a signature of isolation-by-distance along the transect[20].
140 The asymmetric signatures of adaptation we observed in prey and predator may reflect
141 differences in the mechanisms that underlie phenotypic variation in each species. Genes
142 associated with TTX biosynthesis have yet to be discovered; however, toxin production in newts
143 likely requires a complicated biosynthetic pathway. For example, biosynthesis of a similar
144 neurotoxin found in puffer fish, saxitoxin (STX), involves gene expression in a cluster of up to
145 26 genes[21]. Some researchers suggest exogenous factors, like environmentally-derived
146 precursors, may also affect the ability of newts to synthesize or sequester TTX[22,23]. On the other
147 hand, TTX resistance in garter snakes is largely due to a small number of amino acid changes to
148 the p-loops of the $Na_V1.4$ channel[16–19]. These large-effect mutations could make TTX resistance
149 more evolutionarily labile than toxicity, permitting rapid local adaptation in predator
150 populations[5,18].
151 Asymmetric patterns of evolution could also arise from a selective imbalance associated
152 with the interactions between prey and predator. In antagonistic interactions, the species under
153 more intense selection is generally expected to be better adapted to local conditions[24]. While
154 prey are typically thought to experience stronger selection than their predators (the “life-dinner

155 principle”)[25], this asymmetry may be reversed when prey contain deadly toxins like TTX[1]. In
156 fact, populations in central Oregon are the most toxic newts known[5], so non-resistant predators
157 should experience severe fitness consequences.

158 Non-adaptive processes of drift and gene flow provide a parsimonious explanation for
159 landscape-wide variation in newt TTX across the geographic mosaic, but the extreme levels of
160 prey toxin and predator resistance in some locations, such as hotspots like central Oregon, are
161 likely a result of reciprocal arms race coevolution. Outside of hotspots, in regions like northern
162 Washington, divergent selection may even favor a reduction in TTX (i.e., “coldspots”), such that
163 the tight spatial correlation we observed between newt TTX and neutral SNPs reflects gene flow
164 homogenizing variation between cold- and hotspots. This pattern underscores the important role
165 of “trait remixing”, a largely untested component of the geographic mosaic theory that is thought
166 to generate spatial variation in species interactions[3,6]. The neutral processes of drift and gene
167 flow are predicted to continually alter the spatial distribution of allelic and phenotypic variation,
168 potentially interfering with local selection. Gene flow outwards from hotspots of coevolution is
169 predicted to alter dynamics in surrounding populations[26,27], and if gene flow is high, the
170 population with the strongest reciprocal effects on fitness is expected to dictate broader
171 landscape patterns of trait variation[24,26,28]. The homogenizing effects of gene flow may be less
172 influential in snake populations due to the simple genetic basis of TTX resistance and/or strong
173 selection on predators.

174 Our results highlight how not all landscape patterns of phenotypic matching in natural
175 enemies may be the inherent result of coevolution[3]. External factors such as abiotic conditions[29],
176 evolutionary constraints[30], or interactions with other species[31] are likely to have unique effects on
177 the evolution of prey and predator. In the geographic mosaic of arms race coevolution, it appears

178 that phenotypic divergence in newt toxin in disproportionally the result of population structure, a
179 pattern that underlies landscape-wide variation in the armaments of both species. Ultimately, the
180 evolutionary response to selection at the phenotypic interface is almost certain to differ in two
181 interacting species—so much so that coevolution may not always be the most parsimonious
182 explanation for observed patterns of phenotypic divergence and trait matching across the
183 geographic mosaic.

184 **References:**

185 1. Brodie III, E. D. & Brodie, Jr., E. D. Predator-prey arms races. *BioScience* **49**, 557–568
186 (1999).

187 2. Janzen, D. H. When is it coevolution? *Evolution* (1980).

188 3. Gomulkiewicz, R. *et al.* Dos and don'ts of testing the geographic mosaic theory of
189 coevolution. *Heredity* **98**, 249–258 (2007).

190 4. Brodie, Jr., E. D., Ridenhour, B. J. & Brodie III, E. D. The evolutionary response of
191 predators to dangerous prey: hotspots and coldspots in the geographic mosaic of coevolution
192 between garter snakes and newts. *Evolution* **56**, 2067–2082 (2002).

193 5. Hanifin, C. T., Brodie, Jr., E. D. & Brodie III, E. D. Phenotypic mismatches reveal escape
194 from arms-race coevolution. *PLoS Biol* **6**, e60 (2008).

195 6. Thompson, J. N. *The Geographic Mosaic of Coevolution*. (University of Chicago Press,
196 2005).

197 7. Brodie III, E. D. & Ridenhour, B. J. Reciprocal selection at the phenotypic interface of
198 coevolution. *Integr. Comp. Biol.* **43**, 408–418 (2003).

199 8. Benkman, C. W., Parchman, T. L., Favis, A. & Siepielski, A. M. Reciprocal selection causes
200 a coevolutionary arms race between crossbills and lodgepole pine. *Am. Nat.* **162**, 182–194
201 (2003).

202 9. Zangerl, A. R. & Berenbaum, M. R. Phenotype matching in wild parsnip and parsnip
203 webworms: causes and consequences. *Evolution* **57**, 806–815 (2003).

204 10. Toju, H., Ueno, S., Taniguchi, F. & Sota, T. Metapopulation structure of a seed-predator
205 weevil and its host plant in arms race coevolution. *Evolution* **65**, 1707–1722 (2011).

206 11. Lively, C. M. & Dybdahl, M. F. Parasite adaptation to locally common host genotypes.
207 *Nature* **405**, 679 (2000).

208 12. Thrall, P. H., Burdon, J. & Bever, J. D. Local adaptation in the *Linum marginale—*
209 *Melampsora lini* host-pathogen interaction. *Evolution* **56**, 1340–1351 (2002).

210 13. Swenson, N. G., Howard, D. J., Hellberg, A. E. M. E. & Losos, E. J. B. Clustering of contact
211 zones, hybrid zones, and phylogeographic breaks in North America. *Am. Nat.* **166**, 581–591
212 (2005).

213 14. Fozzard, H. A. & Lipkind, G. M. The tetrodotoxin binding site is within the outer vestibule
214 of the sodium channel. *Mar. Drugs* **8**, 219–234 (2010).

215 15. Tikhonov, D. B. & Zhorov, B. S. Architecture and pore block of Eukaryotic voltage-gated
216 sodium channels in view of NavAb bacterial sodium channel structure. *Mol. Pharmacol.* **82**,
217 97–104 (2012).

218 16. Geffeney, S., Brodie, Jr., E. D., Ruben, P. C. & Brodie III, E. D. Mechanisms of adaptation
219 in a predator-prey arms race: TTX-resistant sodium channels. *Science* **297**, 1336–1339
220 (2002).

17. Geffeney, S. L., Fujimoto, E., Brodie III, E. D., Brodie, Jr., E. D. & Ruben, P. C. Evolutionary diversification of TTX-resistant sodium channels in a predator-prey interaction. *Nature* **434**, 759–763 (2005).

18. Feldman, C. R., Brodie, Jr., E. D., Brodie III, E. D. & Pfrender, M. E. Genetic architecture of a feeding adaptation: garter snake (*Thamnophis*) resistance to tetrodotoxin bearing prey. *Proc. R. Soc. B Biol. Sci.* **277**, 3317–3325 (2010).

19. Hague, M. T. J., Feldman, C. R., Brodie, Jr., E. D. & Brodie III, E. D. Convergent adaptation to dangerous prey proceeds through the same first-step mutation in the garter snake *Thamnophis sirtalis*. *Evolution* **71**, 1504–1518 (2017).

20. Ridenhour, B. J., Brodie, Jr., E. D. & Brodie III, E. D. Patterns of genetic differentiation in *Thamnophis* and *Taricha* from the Pacific Northwest. *J. Biogeogr.* **34**, 724–735 (2007).

21. Moczydlowski, E. G. The molecular mystique of tetrodotoxin. *Toxicon* **63**, 165–183 (2013).

22. Yotsu, M., Iorizzi, M. & Yasumoto, T. Distribution of tetrodotoxin, 6-epitetrodotoxin, and 11-deoxytetrodotoxin in newts. *Toxicon* **28**, 238–241 (1990).

23. Yasumoto, T. & Yotsu-Yamashita, M. Chemical and etiological studies on tetrodotoxin and its analogs. *Toxin Rev.* **15**, 81–90 (1996).

24. Gandon, S. Local adaptation and the geometry of host–parasite coevolution. *Ecol. Lett.* **5**, 246–256 (2002).

25. Dawkins, R. & Krebs, J. R. Arms races between and within species. *Proc. R. Soc. Lond. B Biol. Sci.* **205**, 489–511 (1979).

26. Gomulkiewicz, R., Thompson, J. N., Holt, R. D., Nuismer, Scott L. & Hochberg, M. E. Hot spots, cold spots, and the geographic mosaic theory of coevolution. *Am. Nat.* **156**, 156–174 (2000).

27. Thompson, J. N., Nuismer, S. L. & Gomulkiewicz, R. Coevolution and maladaptation. *Integr. Comp. Biol.* **42**, 381–387 (2002).

28. Gandon, S. & Michalakis, Y. Local adaptation, evolutionary potential and host–parasite coevolution: interactions between migration, mutation, population size and generation time. *J. Evol. Biol.* **15**, 451–462 (2002).

29. Johnson, S. G., Hulsey, C. D. & León, F. J. G. Spatial mosaic evolution of snail defensive traits. *BMC Evol. Biol.* **7**, 1–11 (2007).

30. Hague, M. T. J. *et al.* Large-effect mutations generate trade-off between predatory and locomotor ability during arms race coevolution with deadly prey. *Evol. Lett.* **2**, 406–416 (2018).

31. Benkman, C. W., Holimon, W. C. & Smith, J. W. The influence of a competitor on the geographic mosaic of coevolution between crossbills and lodgepole pine. *Evolution* **55**, 282–294 (2001).

32. Gall, B. G. *et al.* Tetrodotoxin levels in larval and metamorphosed newts (*Taricha granulosa*) and palatability to predatory dragonflies. *Toxicon* **57**, 978–983 (2011).

33. Stokes, A. N., Williams, B. L. & French, S. S. An improved competitive inhibition enzymatic immunoassay method for tetrodotoxin quantification. *Biol. Proced. Online* **14**, 3 (2012).

34. Hanifin, C. T., Brodie III, E. D. & Brodie, Jr., E. D. Tetrodotoxin levels of the rough-skin newt, *Taricha granulosa*, increase in long-term captivity. *Toxicon* **40**, 1149–1153 (2002).

35. Hanifin, C. T., Brodie III, E. D. & Brodie, Jr., E. D. A predictive model to estimate total skin tetrodotoxin in the newt *Taricha granulosa*. *Toxicon* **43**, 243–249 (2004).

36. Hague, M. T. J. *et al.* Toxicity and population structure of the Rough-Skinned Newt (*Taricha granulosa*) outside the range of an arms race with resistant predators. *Ecol. Evol.* **6**, 2714–2724 (2016).

37. Murray, S. A., Mihali, T. K. & Neilan, B. A. Extraordinary conservation, gene loss, and positive selection in the evolution of an ancient neurotoxin. *Mol. Biol. Evol.* **28**, 1173–1182 (2010).

38. Brodie III, E. D. & Brodie, Jr., E. D. Tetrodotoxin resistance in garter snakes: an evolutionary response of predators to dangerous prey. *Evolution* **44**, 651–659 (1990).

39. Ridenhour, B. J., Brodie III, E. D. & Brodie, Jr., E. D. Resistance of neonates and field-collected garter snakes (*Thamnophis* spp.) to tetrodotoxin. *J. Chem. Ecol.* **30**, 143–154 (2004).

40. Ridenhour, B. The coevolutionary process: The effects of population structure on a predator-prey system. (Indiana University, 2004).

41. Lynch, M., Walsh, B. & others. *Genetics and analysis of quantitative traits*. **1**, (Sinauer Sunderland, MA, 1998).

42. Bates, D., Mächler, M., Bolker, B. & Walker, S. Fitting linear mixed-effects models using lme4. *J. Stat. Softw.* **67**, 1–48 (2015).

43. Cumming, G. & Finch, S. Inference by eye: Confidence intervals and how to read pictures of data. *Am. Psychol.* **60**, 170–180 (2005).

44. Vicoso, B., Emerson, J., Zektser, Y., Mahajan, S. & Bachtrog, D. Comparative sex chromosome genomics in snakes: differentiation, evolutionary strata, and lack of global dosage compensation. *PLoS Biol.* **11**, e1001643 (2013).

45. Augstenová, B. *et al.* ZW, XY, and yet ZW: Sex chromosome evolution in snakes even more complicated. *Evolution* **72**, 1701–1707 (2018).

46. Stephens, M., Smith, N. J. & Donnelly, P. A new statistical method for haplotype reconstruction from population data. *Am. J. Hum. Genet.* **68**, 978–989 (2001).

47. Graffelman, J. & Morales-Camarena, J. Graphical tests for Hardy-Weinberg Equilibrium based on the ternary plot. *Hum. Hered.* **65**, 77–84 (2008).

48. Graffelman, J. & Weir, B. S. Multi-allelic exact tests for Hardy–Weinberg equilibrium that account for gender. *Mol. Ecol. Resour.* **18**, 461–473 (2018).

49. Graffelman, J. & Weir, B. S. On the testing of Hardy-Weinberg proportions and equality of allele frequencies in males and females at biallelic genetic markers. *Genet. Epidemiol.* **42**, 34–48 (2018).

50. Graffelman, J. & Weir, B. Testing for Hardy–Weinberg equilibrium at biallelic genetic markers on the X chromosome. *Heredity* **116**, 558 (2016).

51. Excoffier, L. & Lischer, H. E. L. Arlequin suite ver 3.5: a new series of programs to perform population genetics analyses under Linux and Windows. *Mol. Ecol. Resour.* **10**, 564–567 (2010).

52. Hanifin, C. T., Yotsu-Yamashita, M., Yasumoto, T. & Brodie, E. D. Toxicity of dangerous prey: variation of tetrodotoxin levels within and among populations of the newt *Taricha granulosa*. *J. Chem. Ecol.* **25**, 2161–2175 (1999).

53. Williams, B. L., Brodie, E. D. & Brodie, E. D. Comparisons between toxic effects of tetrodotoxin administered orally and by intraperitoneal injection to the garter snake *Thamnophis sirtalis*. *J. Herpetol.* **36**, 112–115 (2002).

54. Brodie III, E. D. & Brodie, Jr., E. D. Evolutionary response of predators to dangerous prey: reduction of toxicity of newts and resistance of garter snakes in island populations. *Evolution* **45**, 221–224 (1991).

55. Williams, B. L., Brodie, Jr., E. D. & Brodie III, E. D. Coevolution of deadly toxins and predator resistance: self-assessment of resistance by garter snakes leads to behavioral rejection of toxic newt prey. *Herpetologica* **59**, 155–163 (2003).

56. Williams, B. L., Hanifin, C. T., Brodie, Jr., E. D. & Brodie III, E. D. Tetrodotoxin affects survival probability of rough-skinned newts (*Taricha granulosa*) faced with TTX-resistant garter snake predators (*Thamnophis sirtalis*). *Chemoecology* **20**, 285–290 (2010).

57. Peterson, B. K., Weber, J. N., Kay, E. H., Fisher, H. S. & Hoekstra, H. E. Double digest RADseq: An inexpensive method for de novo SNP discovery and genotyping in model and non-model species. *PLoS ONE* **7**, e37135–11 (2012).

58. Andrew, S. *FastQC*. (2016).

59. Catchen, J., Hohenlohe, P. A., Bassham, S., Amores, A. & Cresko, W. A. Stacks: an analysis tool set for population genomics. *Mol. Ecol.* **22**, 3124–3140 (2013).

60. Langmead, B. & Salzberg, S. L. Fast gapped-read alignment with Bowtie 2. *Nat. Methods* **9**, 357–359 (2012).

61. Gruber, B., Unmack, P. J., Berry, O. F. & Georges, A. dartr: An r package to facilitate analysis of SNP data generated from reduced representation genome sequencing. *Mol. Ecol. Resour.* (2017).

62. R Core Team. *R: A Language and Environment for Statistical Computing*. (R Foundation for Statistical Computing, 2018).

63. Foll, M. & Gaggiotti, O. A genome-scan method to identify selected loci appropriate for both dominant and codominant markers: a Bayesian perspective. *Genetics* **180**, 977–993 (2008).

64. Nei, M. *Molecular evolutionary genetics*. (Columbia University Press, 1987).

65. Goudet, J. & Jombart, T. *hierfstat: Estimation and Tests of Hierarchical F-Statistics*. (2015).

66. Weir, B. S. & Cockerham, C. C. Estimating F-statistics for the analysis of population structure. *evolution* **38**, 1358–1370 (1984).

338 67. Pembleton, L. W., Cogan, N. O. I. & Forster, J. W. StAMPP: an R package for calculation of
339 genetic differentiation and structure of mixed-ploidy level populations. *Mol. Ecol. Resour.*
340 **13**, 946–952 (2013).

341 68. Rousset, F. Genetic differentiation and estimation of gene flow from F-statistics under
342 isolation by distance. *Genetics* **145**, 1219–1228 (1997).

343 69. Legendre, P. & Fortin, M.-J. Comparison of the Mantel test and alternative approaches for
344 detecting complex multivariate relationships in the spatial analysis of genetic data. *Mol.*
345 *Ecol. Resour.* **10**, 831–844 (2010).

346 70. Meirmans, P. G. Seven common mistakes in population genetics and how to avoid them.
347 *Mol. Ecol.* **24**, 3223–3231 (2015).

348 71. Oksanen, J. *et al. vegan: Community Ecology Package*. (2018).

349 72. Pritchard, J. K., Stephens, M. & Donnelly, P. Inference of population structure using
350 multilocus genotype data. *Genetics* **155**, 945–959 (2000).

351 73. Falush, D., Stephens, M. & Pritchard, J. K. Inference of population structure using
352 multilocus genotype data: linked loci and correlated allele frequencies. *Genetics* **164**, 1567–
353 1587 (2003).

354 74. Earl, D. A. & vonHoldt, B. M. STRUCTURE HARVESTER: a website and program for
355 visualizing STRUCTURE output and implementing the Evanno method. *Conserv. Genet.*
356 *Resour.* **4**, 359–361 (2012).

357 75. Evanno, G., Regnaut, S. & Goudet, J. Detecting the number of clusters of individuals using
358 the software structure: a simulation study. *Mol. Ecol.* **14**, 2611–2620 (2005).

359 76. Jakobsson, M. & Rosenberg, N. A. CLUMPP: a cluster matching and permutation program
360 for dealing with label switching and multimodality in analysis of population structure.
361 *Bioinformatics* **23**, 1801–1806 (2007).

362 77. Francis, R. M. pophelper: An R package and web app to analyse and visualise population
363 structure. *Mol. Ecol. Resour.* **17**, 27–32 (2017).

364 78. Manly, B. F. J. Randomization and regression methods for testing for associations with
365 geographical, environmental and biological distances between populations. *Res. Popul. Ecol.*
366 **28**, 201–218 (1986).

367 79. Smouse, P. E., Long, J. C. & Sokal, R. R. Multiple regression and correlation extensions of
368 the mantel test of matrix correspondence. *Syst. Zool.* **35**, 627 (1986).

369 80. Legendre, P., Lapointe, F.-J. & Casgrain, P. Modeling brain evolution from behavior: a
370 permutational regression approach. *Evolution* **48**, 1487–1499 (1994).

371 81. Lichstein, J. W. Multiple regression on distance matrices: a multivariate spatial analysis tool.
372 *Plant Ecol.* **188**, 117–131 (2007).

373 82. Rosenblum, E. B. Convergent evolution and divergent selection: lizards at the White Sands
374 ecotone. *Am. Nat.* (2005).

375 83. Raufaste, N. & Rousset, F. Are partial mantel tests adequate? *Evolution* **55**, 1703–1705
376 (2001).

84. Rousset, F. & Waller, D. Partial Mantel tests: reply to Castellano and Balletto. *Evolution* **56**, 1874–1875 (2002).

85. Szymura, J. M. & Barton, N. H. Genetic analysis of a hybrid zone between the fire-bellied toads, *Bombina bombina* and *B. variegata*, near Cracow in southern Poland. *Evolution* **40**, 1141–1159 (1986).

86. Szymura, J. M. & Barton, N. H. The genetic structure of the hybrid zone between the fire-bellied toads *Bombina bombina* and *B. variegata*: comparisons between transects and between loci. *Evolution* **45**, 237–261 (1991).

87. Derryberry, E. P., Derryberry, G. E., Maley, J. M. & Brumfield, R. T. HZAR: hybrid zone analysis using an R software package. *Mol. Ecol. Resour.* **14**, 652–663 (2014).

88. Baldassarre, D. T., White, T. A., Karubian, J. & Webster, M. S. Genomic and morphological analysis of a semipermeable avian hybrid zone suggests asymmetrical introgression of a sexual signal. *Evolution* **68**, 2644–2657 (2014).

89. Scordato, E. S. *et al.* Genomic variation across two barn swallow hybrid zones reveals traits associated with divergence in sympatry and allopatry. *Mol. Ecol.* **26**, 5676–5691 (2017).

90. Fox, J. & Weisberg, S. *An R companion to applied regression*. (Sage, 2011).

91. Nakagawa, S. & Schielzeth, H. A general and simple method for obtaining R^2 from generalized linear mixed-effects models. *Methods Ecol. Evol.* **4**, 133–142 (2013).

92. Bartoń, K. *MuMIn: Multi-Model Inference*. (2018).

Acknowledgements:

We thank the Departments of Fish and Wildlife in Washington and Oregon for scientific collecting permits to MTJH (18-082 and 063-18, respectively). We also thank IACUC for the protocol to EDB, Jr. at USU (1008). We are grateful for T. St. Pierre's help with fieldwork. J. McGlothlin and K. Gendreau helped with sex-linked analyses of $Na_V1.4$ and provided valuable feedback that improved the quality of this manuscript. R. Cox, D. Taylor, A. Bergland, D. Carr, and the Brodie and Feldman lab groups also provided helpful input. **Funding**: This work was supported by a Doctoral Dissertation Improvement Grant from the National Science Foundation to MTJH and EDB III (DEB 1601296) and NSF support to EDB III (DEB 0922251). **Author contributions**: MTJH designed the project, collected specimens, generated genetic data, and performed statistical analyses. ANS collected phenotypic data on newt TTX levels. CRF collected specimens and phenotypic data on snake resistance. EDB, Jr. collected phenotypic data on snake resistance and provided leadership on the project. EDB III designed the project and provided leadership. All authors prepared the manuscript. **Competing interests**: The authors declare no conflict of interest with this manuscript.

Fig. 1. Matching phenotypes in prey and predator imply local co-adaptation in the arms race. (**A**) Population means of TTX levels (μg/cm^2) in newts and (**B**) phenotypic TTX resistance (50% MAMU dose) in snakes along the latitudinal transect. Error bars indicate 95% confidence intervals. The x-axis represents linear distance (km) from the northernmost sampling site (Clallam; 0 km). For snakes, the frequency of TTX-resistant alleles in the $Na_V1.4$ channel is shown with pie charts proportional to sample size. To the right, the schematic of $Na_V1.4$ shows the four domains of the channel (DI–DIV), with the extracellular pore loops (p-loops) highlighted with bold lines. Specific amino acid changes in the DIV p-loop are shown in their relative positions within the pore. The TTX-sensitive ancestral sequence (purple) is listed, followed by the two derived alleles known to confer increases in channel resistance in this lineage. (**C**) Map inset illustrates population estimates of prey toxin and predator resistance at each location in the geographic mosaic. Blue colors correspond to low estimates of TTX (squares) or resistance (circles), whereas red indicates escalated phenotypes in the arms race.

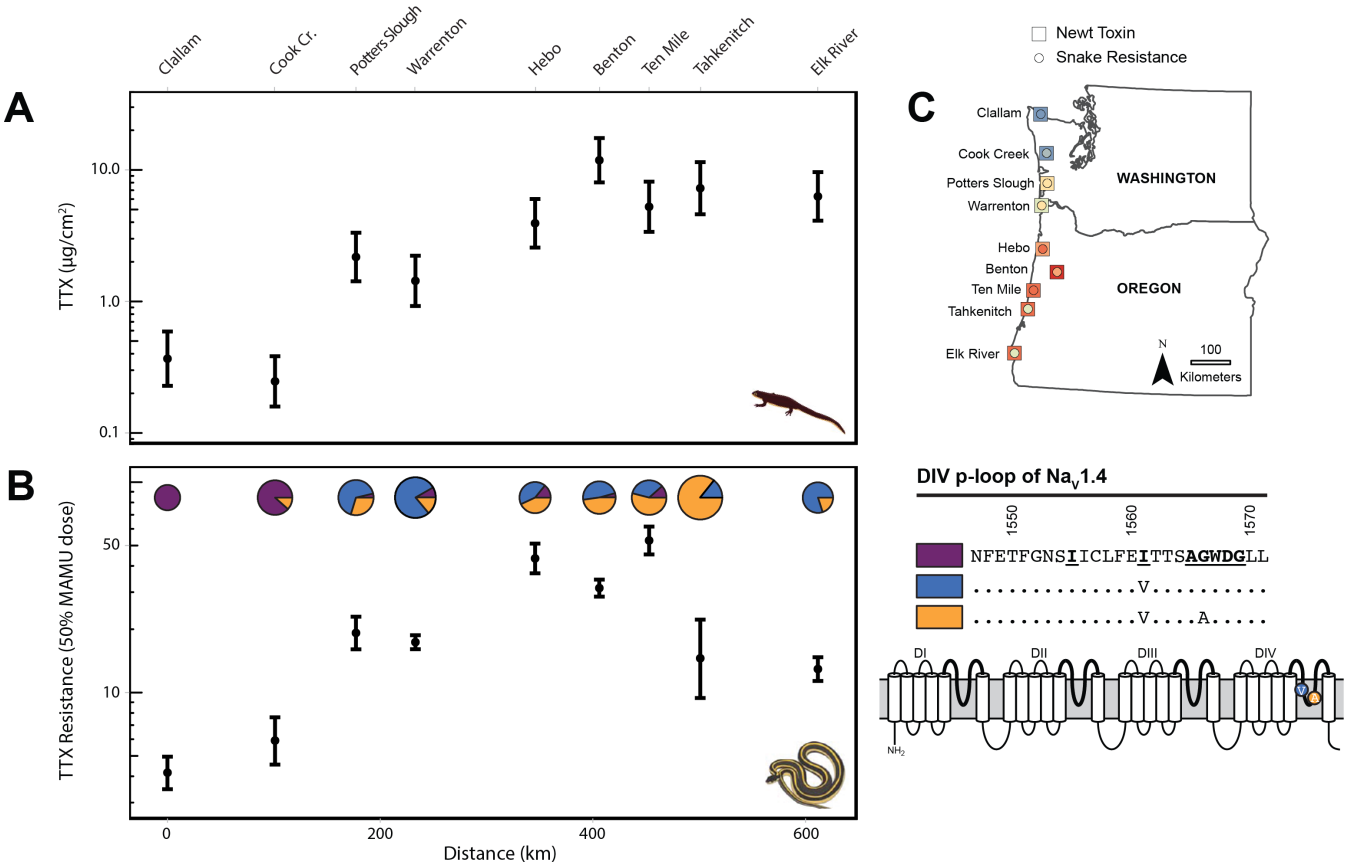

Fig. 2. Populations of prey and predator differ in geographic structure. Results from the principal coordinate (PCoA) and STRUCTURE analyses of neutral SNPs from newts and snakes. PCoA graphs are rotated 90º to emphasize the major axis of variation corresponding to latitude. The PC 1 values for each individual were used as a neutral expectation in the cline-fitting analyses. STRUCTURE plots are arranged latitudinally by population, in the same order as the map. Each horizontal bar represents the ancestry assignment of an individual, with populations separated by white dashed lines.

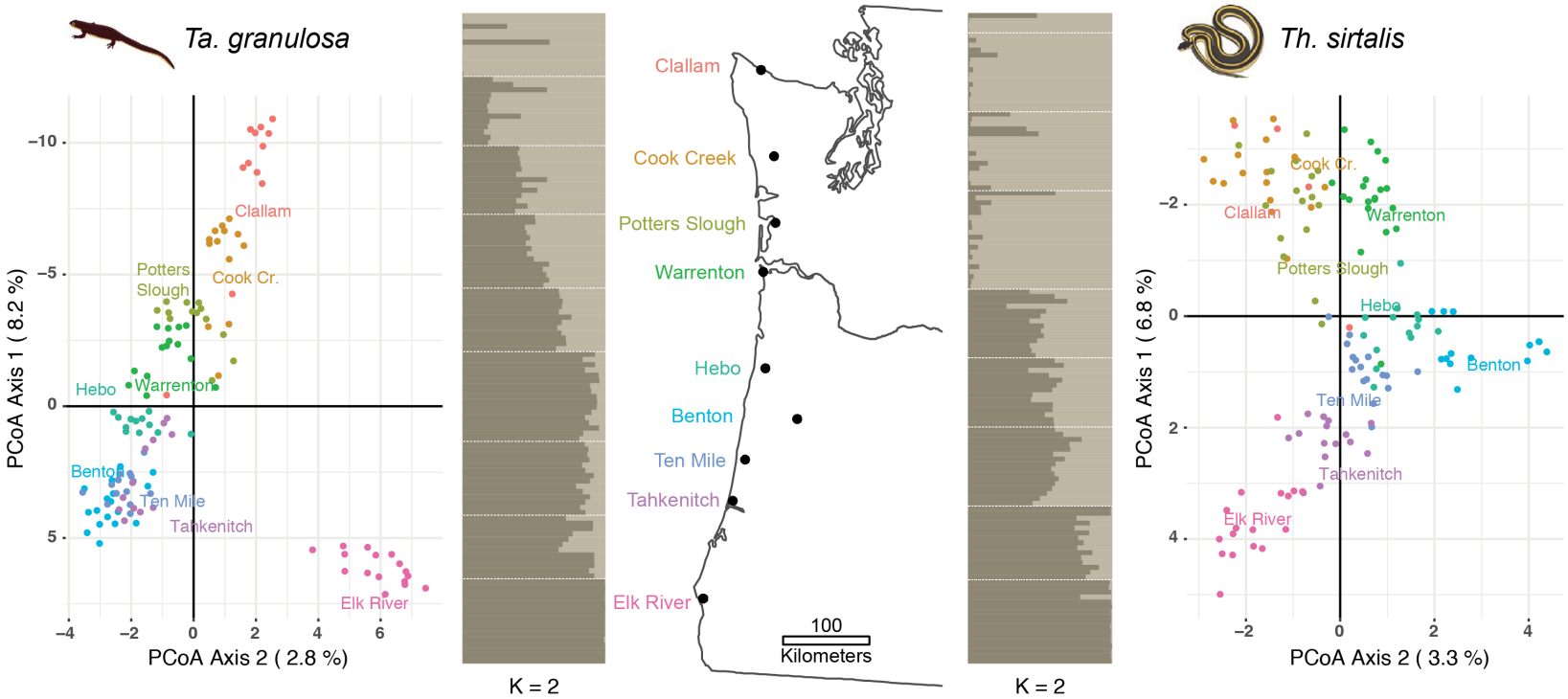

Fig. 3. Levels of prey toxin are best predicted by neutral population structure, whereas predator resistance is predicted by prey toxin. Cline-fitting results for phenotypic and genetic variation are shown, with error bars indicating confidence intervals surrounding the geographic cline centers. (**A**) Phenotypic clines of TTX levels (log[TTX μg/cm^2 + 0.1]) and (**B**) TTX resistance (ln[MAMU + 1]) are shown in red. For snakes, the frequency of TTX-resistant alleles in the $Na_V1.4$ channel was also modeled (in black). Gray dashed lines represent the neutral expectation for trait variation due to population structure, based on the PCoA. The cline center points of TTX levels and neutral PC 1 in newts, and phenotypic resistance and TTX-resistant alleles in snakes, are all located within in 84 km of each other along the 611 km transect.

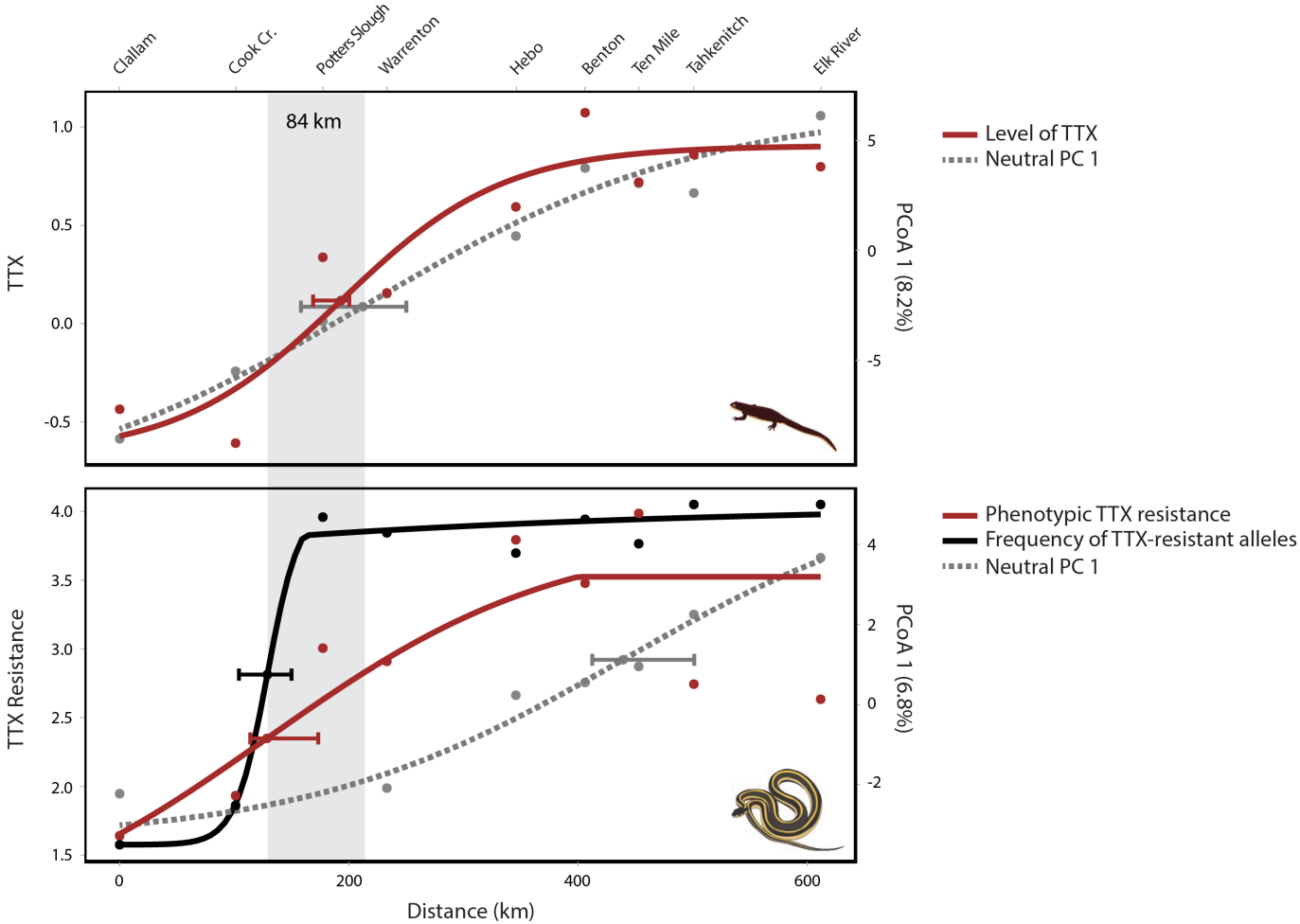

437 **Table 1.** Results from multiple regression of distance matrices (MRMs) comparing population
438 divergence in phenotypic and genetic data.
439

Response Variable	Explanatory Variable(s)	Coefficient	p-value	R^2
Newt TTX levels	Neutral F_{ST} of newts	5.998	**0.002***	0.414
	TTX resistance of snakes	0.415	**0.019***	0.274
	Neutral F_{ST} + TTX resistance			
	Neutral F_{ST} of newts	4.827	**0.006***	0.501
	TTX resistance of snakes	0.253	0.065˙	
Snake TTX resistance	Neutral F_{ST} of snakes	1.442	0.719	0.006
	TTX level of newts	0.662	**0.021***	0.274
	Neutral F_{ST} + TTX toxicity			
	Neutral F_{ST} of snakes	-5.830	0.189	0.338
	TTX level of newts	0.873	**0.011***	
	Neutral F_{ST} of newts	4.632	**0.035***	0.155
Snake F_{ST} of DIV p-loop	Neutral F_{ST} of snakes	2.649	0.202	0.080
	Neutral F_{ST} of newts	3.196	**0.010***	0.311

440

441 **Methods:**

442 We sampled phenotypic and genomic data from *Ta. granulosa* (*n*=138) and *Th. sirtalis*
443 (*n*=169) at nine locations along a latitudinal transect in the states of Washington and Oregon
444 (Fig. 1; Supplementary Table S1) and compared mosaic patterns of escalation in the arms race to
445 neutral population genomic structure across the landscape. We chose to focus our analysis on
446 populations of *Ta. granulosa* and *Th. sirtalis* in the Pacific Northwest of North America. Other
447 regions of sympatry, particularly in California, contain additional TTX-bearing newt species
448 (e.g., *Ta. torosa*) and resistant garter snakes (e.g., *Th. atratus*), which could confound inferences
449 of coevolution between specific species pairs.

450

451 *TTX levels of* Taricha granulosa

452 We estimated levels of TTX in *Ta. granulosa* using a Competitive Inhibition Enzymatic
453 Immunoassay (CIEIA) and TTX-specific antibodies[32,33]. We quantified the amount of TTX in a
454 5mm circular skin punch from the dorsum of each newt using a human skin-biopsy punch (Acu-
455 Punche, Acuderm Inc.)[34–36]. These data were used to estimate the dorsal skin concentration of
456 TTX ($\mu g/cm^2$) in each individual. TTX is uniformly distributed throughout the dorsum and levels
457 of TTX in the dorsal skin are tightly correlated with toxicity in other regions[35]. We conducted a
458 two-way ANOVA to test whether TTX differed by population and by sex, because past work
459 suggests toxin levels may vary by sex[34]. Distribution and leverage analyses indicated that a log(x
460 + 0.1) transformation of TTX was needed. Transformed mean and variance values were used in
461 the cline-fitting analysis of TTX along the transect.

462 Although a considerable body of work has described the genetic basis of TTX resistance
463 in *Th. sirtalis* (see below), similar information regarding TTX in *Ta. granulosa* is unavailable.

464 Although we were unable to characterize genetic variation underlying prey toxin, we assume that
465 TTX production probably has a polygenic basis. For example, biosynthesis of saxitoxin (STX), a
466 similar neurotoxin found in marine species, involves gene expression in a cluster of up to 26
467 genes in cyanobacteria[37].
468
469 *TTX resistance of* Thamnophis sirtalis
470 We measured phenotypic TTX resistance using a well-established bioassay of whole
471 animal performance[4,19,38,39]. Briefly, each individual was assayed on a 4 m racetrack to
472 characterize its "baseline" crawl speed, then injected intraperitoneally with a known dose of TTX
473 and assayed for "post-injection" speed. Population estimates of phenotypic TTX resistance are
474 reported on a scale of mass-adjusted mouse units (MAMUs) to control for differences in body
475 size[4]. Resistance was estimated as the relative performance after injection: the MAMU dose of
476 TTX that reduces performance by 50% of baseline speed. We incorporated racetrack data from
477 previously published estimates of resistance from the same sampling locations to generate
478 precise population estimates of phenotypic resistance in this study (see Supplementary Table
479 S1)[4,40].
480 The 50% MAMU dose was estimated separately for each population from a dose-
481 response curve using curvilinear regression and the general transform $y' = \ln(1/y - 1)$[4]. Individuals
482 from each population received a series of TTX doses, with an average of 2.5 different doses per
483 individual. At y=0.5 (i.e., 50%), y'=0 and the 50% dose is estimable $\hat{x} = -\alpha/\beta$ (where α is the
484 intercept and β the slope from the curvilinear regression). Because $\hat{x}$ takes the form of a ratio,
485 the standard error for the estimated 50% dose is calculated using standard methods for the
486 variance of a ratio[4,41]. Confidence intervals of 95% were calculated as ±1.96 SE. Regression was

487 performed in R with the "lmer" function implemented in the lme4 package[42]. The individual ID
488 of each snake was included as a random effect to account for the fact that each snake received
489 multiple injections. Distribution and leverage analysis indicated that a transformation of the x
490 variable (MAMU of TTX) was needed, so we transformed the data using $x' = \ln(x + 1)$[4].
491 Differences among populations in phenotypic TTX resistance were deemed significant if 95%
492 confidence intervals did not overlap by more than half of a one-sided error bar[43].
493 We genotyped snakes for their amino acid sequence in the DIV p-loop of the $Na_V1.4$
494 channel. Methods for Sanger sequencing are described in Hague et al. (2017)[19]. For each
495 individual, we sequenced a 666 bp fragment that includes the DIV p-loop region of $Na_V1.4$. The
496 $Na_V1.4$ protein is encoded by the *SCN4A* gene located on the Z sex chromosome of *Th. sirtalis*
497 (Gendreau et al., *in prep*). Colubrid snakes, including garter snakes, have heteromorphic sex
498 chromosomes (ZZ males, ZW females) that are non-recombining[44,45], and females appear to be
499 hemizygous for the Z-linked *SCN4A* gene. We used sex-specific PCR primers to confirm the sex
500 of each individual (ZW.734.F, 5'-TAAGGTCCTGGGCATGTCCT-3'; ZW.2468.R, 5'-
501 ATGGCTTGGAATGAGGTGGG-3'; Gendreau et al., *in prep*). In DIV p-loop sequences from
502 males, heterozygous positions on chromatograms were identified by eye and confirmed in both
503 directions with sequencing. The haplotype phase of the DIV p-loop sequence for each male was
504 inferred computationally with the program PHASE[46].
505 We translated the aligned DIV p-loop coding sequences into the amino acids and tested
506 for departures from Hardy-Weinberg Equilibrium (HWE) using a joint test for HWE and
507 equality of allele frequencies (EAF) using the *HWTriExact* function in the HardyWeinberg
508 package in R[47–49]. Standard tests for HWE rely on the assumption of EAF in males and females.
509 The joint exact test for HWE and EAF accounts for the hemizygous sex and tests for joint

510 departures of HWE and EAF[48–50]. We also calculated pairwise F_{ST} divergence at the DIV p-loop
511 in the program Arlequin[51] and used a Mantel test to test for a relationship between pairwise F_{ST}
512 divergence at the DIV p-loop and phenotypic divergence in whole-animal TTX resistance.
513 Significance was tested with 1000 permutations.
514
515 *Analysis of phenotypic matching*
516 Following Hanifin et al. (2008)[5], we estimated functional levels of newt TTX and snake
517 resistance to visualize whether prey and predator exhibit matched levels of escalation along the
518 transect. The model provides a rough estimate of functional interactions between newt TTX and
519 snake resistance based on an extensive body of work[4,7,35,38,39,52–54]. Localities are considered
520 "matched" if a sympatric interaction between prey and predator could potentially result in
521 variable fitness outcomes for both species, leading to reciprocal selection between newt TTX and
522 snake resistance[5]. For each locality, we estimated whole-newt levels of TTX (mg) and the dose
523 of TTX (mg) required to reduce performance of co-occurring snakes to 15%, 50%, and 85% of
524 their baseline performance. The TTX dose required to reduce snake performance by 50% is
525 considered a perfect functional match between newt TTX and snake resistance. The 15% and
526 85% doses delimit the range of functionally relevant doses for snakes. At performance levels
527 <15%, all snakes that ingest newts are fully immobilized or killed and newts escape, whereas at
528 performance levels >85% all snakes are unaffected and captured newts die[5,55,56]. Localities where
529 the full range of TTX doses found in newts fall outside the 15-85% region of phenotypic space
530 are considered phenotypic "mismatches", such that variable fitness outcomes and reciprocal
531 selection are unlikely to occur.

532 Methods for estimating functionally comparable values of newt TTX and snake
533 resistance are described in Hanifin et al. (2008)[5]. Briefly, we extrapolated our measures of newt
534 TTX in skin samples ($\mu g/cm^2$) to the whole animal (mg of TTX/newt) using standard methods.
535 For snakes, the 15, 50, and 85% MAMU doses were extracted from the dose response curves of
536 each population (as described above). We converted snake resistance from MAMUs based on
537 intraperitoneal (IP) injections to mg of TTX in oral doses using the following equation:

538 $$\text{IPdose(mg)} = (\theta * 0.00001429) * \text{snake mass(g)}$$

539 where θ is the MAMU dose and 0.0001429 is the conversion factor (1 MAMU= 0.01429μg TTX
540 per gram of snake). The effects of TTX are dependent on body size, so we estimated the oral
541 dose of TTX required to slow the average adult *Th. sirtalis* (mean adult mass = 52.84 g). We
542 then converted the IP dose (mg) to the oral dose required to achieve the same performance
543 reduction by multiplying the IP dose by 40. Estimates of orally ingested doses of TTX (mg)
544 required to reduce snake performance by 15, 50, and 85% were used as a functionally equivalent
545 metric to compare predator phenotypes to those of the prey (Supplementary Table S2).
546

547 *ddRADseq library preparation*

548 We prepared ddRADseq libraries separately for *Ta. granulosa* and *Th. sirtalis* using the
549 protocol described in Peterson et al. (2012)[57]. Genomic DNA was extracted using the DNeasy
550 Blood & Tissue kit (Qiagen Inc., Valencia, CA.). We digested 600 ng of genomic DNA for each
551 sample using the restriction enzymes *EcoRI* and *SbfI* for *Ta. granulosa* and *MfeI* and *SbfI* for *Th.*
552 *sirtalis*. Unique combinations of individual P1 and P2 barcoded adapters were annealed to the
553 digested genomic DNA of each sample. Each barcode was six base pairs long and differed by at
554 least two nucleotides. After barcoding, *Ta. granulosa* and *Th. sirtalis* samples were pooled

555 separately, purified with AmpureXP beads (Beckman Coulter, Inc., Brea, CA, USA), and size
556 selected for 500 to 600 bp fragments using a Pippin Prep (Sage Science, Inc., Beverly, MA,
557 USA). We enriched the adapter-ligated fragments in the size-selected libraries using 16 PCR
558 cycles and then purified the product with AmpureXP beads. The *Ta. granulosa* and *Th. sirtalis*
559 libraries were each run on two lanes of the Illumina HiSeq 2500 platform (Illumina, Inc., San
560 Diego, CA, USA) to generate 125 bp paired-end reads.
561
562 *Data processing of Illumina sequencing*
563 Read quality of the raw sequence data was assessed using FastQC 0.11.5[58]. We used
564 *process_radtags* in Stacks 1.46[59] on both the *Ta. granulosa* and *Th. sirtalis* datasets to
565 demultiplex reads and removed sequences with low-quality scores or uncalled bases. For the *Ta.*
566 *granulosa* dataset, we used the *denovo_map.pl* pipeline in Stacks, because a reference genome is
567 not currently available. We used a minimum depth of three (-*m*), a distance of three between
568 stacks (-*M*), and a distance of three between catalog loci (-*n*). The *Th. sirtalis* reads were aligned
569 to the *Th. sirtalis* genome using Bowtie2 2.2.9[60]. We discarded reads that did not align or had
570 more than one match to the genome. We used *ref_map.pl* in Stacks to assemble the reference-
571 aligned sequences into loci, with a minimum depth of three (-*m*). For both species, we used
572 *populations* in Stacks to select loci with a minimum depth of 10x coverage. To avoid linkage
573 among sites within the same locus, we only retained one single nucleotide polymorphism (SNP)
574 per locus.
575 We used the dartR package in R[61,62] to remove loci and individuals with >30% missing
576 data. We also removed loci with a minor allele frequency (MAF) <5%, including those that were
577 invariant. Finally, we removed putative loci under selection. The program BayeScan 2.1 was

578 used to search for loci with F_{ST} coefficients that were significantly different than those expected
579 under neutrality[63]. The Bayesian analysis used 20 pilot runs with 5,000 iterations followed by an
580 additional burn-in of 50,000 and 50,000 output iterations. An outlier analysis with FDR-
581 corrected p-values (q-values) <0.05 was used to identify and remove outlier loci putatively under
582 selection.
583
584 *Analysis of neutral population structure*
585 The filtered SNPs for each species were used to calculate observed heterozygosity (H_O)
586 and gene diversity (H_S) for each population[64] using the hierfstat package in R[65]. To estimate
587 neutral population genomic structure, we calculated global and pairwise F_{ST} values[66]. Confidence
588 intervals were estimated by running 1000 bootstraps over loci using the hierfstat and stAMPP
589 packages in R[67]. We tested for a pattern of isolation-by-distance (IBD) along each transect by
590 performing Mantel tests on matrices of linearized F_{ST} and geographic distance[68]. We also
591 conducted distance-based redundancy analyses (dbRDA), which are thought to be more reliable
592 than Mantel tests at detecting spatial patterns like IBD[69,70]. We conducted dbRDA analyses in the
593 vegan package in R[71] to test for a relationship between pairwise F_{ST} values and the geographic
594 coordinates (latitude and longitude) of sampling locations. We assessed significance of IBD tests
595 with 1000 permutations.
596 We visualized population structure of each species using a principal coordinate analysis
597 (PCoA) in the dartR package in R. The first axis (PC 1) from the PCoA captured latitudinal
598 variation along the transect for both newts and snake (Fig. 2); therefore, we used the PC 1 values
599 for each individual as a neutral expectation in the cline-fitting analyses (see below). We assessed
600 population structure using a Bayesian assignment approach implemented in the program

601 STRUCTURE[72,73]. We estimated the optimal number of genetic clusters (K) ranging for one to
602 nine, without populations included as priors. The model assumed population admixture and
603 correlated allele frequencies[73]. The analysis first ran for 100,000 iterations as burn-in and then
604 we collected data from the following 1,000,000 interactions in 10 different independent runs.
605 STRUCTURE HARVESTER[74] was used to detect the most probable K using the Evanno's
606 method[75]. Ancestry proportion (Q) values of the 10 runs for each value of the most probable K
607 we averaged using CLUMPP[76] and visualized using the pophelper package in R[77]. We calculated
608 the average Q value for each population, which represent the fraction of membership to each
609 genetic cluster (K). These Q estimates were used as a neutral expectation in cline-fitting analyses
610 (see below) and compared to the cline results of PC 1 from the PCoA.
611
612 *Multiple regression of distance matrices (MRMs)*
613 MRMs are an extension of Mantel tests that involve multiple regression of a response
614 distance matrix on explanatory matrices[78–81]. Partial regression coefficients can be used to
615 understand the relationship between two matrices while controlling for the effects of a third
616 matrix[10,82]. For each species, we generated two distance matrices: (1) pairwise phenotypic
617 divergence in the coevolutionary trait (e.g., log-transformed TTX of *Ta. granulosa*) and (2)
618 pairwise genomic divergence (F_{ST}) from neutral SNPs. We then tested whether population
619 patterns of phenotypic escalation in a focal species (e.g., TTX of *Ta. granulosa*) are best
620 explained by neutral genomic divergence (pairwise F_{ST}) or escalation in the natural enemy (TTX
621 resistance of *Th. sirtalis*). MRM analyses can be confounded when explanatory variables are
622 spatially autocorrelated, so we compared results when the two explanatory variables were
623 analyzed separately and together[82–84].

624

625 *Cline analyses*

626 We performed ML cline-fitting analyses on the phenotypic and genetic data from each
627 species[85,86]. For *Ta. granulosa*, we fit a cline to TTX levels using the mean and variance of the
628 log-transformed TTX data (μg/cm^2). For *Th. sirtalis*, we fit (1) a cline to phenotypic TTX
629 resistance using the 50% MAMU dose and variance from the ln-transformed MAMU data and
630 (2) a genetic cline to the frequency of TTX-resistant alleles in each population. Two different
631 TTX-resistant DIV alleles occur in the Pacific Northwest: $Na_V1.4^V$ is generally found at high
632 frequency in the center of the transect, whereas $Na_V1.4^{VA}$ occurs predominately in southern
633 populations (Fig. 1). We generated separate clines for each allele (data not shown), but the cline
634 fit to the combined frequency of both TTX-resistant alleles (Fig. 3) was the most representative
635 of variation along the entire transect. For each species, we compared clinal variation in
636 coevolutionary traits to variation at the neutral SNPs. We first fit clines to the PC 1 values from
637 the PCoA of each species, and secondly, we fit clines to the ancestry proportions (Q) from the
638 most likely value of K for each species (K=2). We reran cline-fitting analyses with the Elk River
639 population removed from the *Ta. granulosa* dataset, because the PCoA (Fig. 2) and
640 STRUCTURE plot of K=3 (Extended Fig. 2) both suggest the population is genetically distinct
641 from all others; however, this produced the same qualitative result as when the population was
642 included.

643 We fit clines using the HZAR package in R[87]. We calculated distances along the cline as
644 kilometers (km) from the northernmost sampling site (Clallam). We ran 15 separate models that
645 varied in the number of cline shape parameters estimated. All models estimated the cline center
646 (distance from sampling location 1, *c*) and width (1/maximum slope, *w*), but could additionally

647 estimate combinations of exponential decay curve (tail) parameters (neither tail, right tail only,
648 left tail only, mirrored tails, or both tails separately), which represent the distance from the cline
649 center to the tail (δ) and the slope of the tail (τ). The genetic models varied as to whether they
650 estimated allele frequencies at the cline ends (p_{min} and p_{max}) or fixed them at 0 and 1. All models
651 were then compared using AIC corrected for small sample sizes (AICc) and maximum likelihood
652 parameters were extracted for the best-fitting model. We considered cline centers with non-
653 overlapping two log-likelihood unit support limits (confidence intervals; CIs) to occur in
654 significantly different geographic locations[88,89].

655 The cline-fitting analyses revealed a tight correlation between the TTX levels of *Ta.*
656 *granulosa* and PC 1 from the PCoA of neutral SNPs (Fig. 3). To further assess this relationship,
657 we fit linear models that tested whether clinal variation in TTX is best explained by neutral
658 population structure from PCs 1 and 2 of the PCoA (model 1) or escalation of TTX resistance in
659 *Th. sirtalis* (model 2). We then fit a combined model including all explanatory variables (model
660 3) to test whether neutral structure from the PCoA predicts TTX levels even after controlling for
661 the TTX resistance of *Th. sirtalis* (Supplementary Table S6).

662 We conducted an analogous set of tests (models 1-3) for *Th. sirtalis* to assess whether
663 TTX resistance is best predicted by neutral structure from the PCoA or the TTX levels of *Ta.*
664 *granulosa*; however, the analyses were more complicated because population estimates of TTX
665 resistance (50% MAMU doses) are extracted from a dose response curve. TTX resistance of
666 individual snakes is measured as a proportion (i.e., the reduction in crawl speed after a given
667 dose of TTX), with each individual receiving multiple injections. We accounted for these data by
668 fitting linear mixed models using the "lmer" function in the R package *lme4*[42]. We treated "post-
669 injection" crawl speed (after a given dose of TTX) as the response variable, and included

670 “baseline” crawl speed and the dose of TTX as covariates in each model. We also included
671 individual ID as a random effect to account for the fact that individuals received multiple doses.
672 Post-injection crawl speed was log-transformed to account for non-normality. Statistical
673 significance of fixed effects was determined by an ANOVA using a Wald Chi-Square test with
674 type III sum of squares and one degree of freedom, implemented in the *car* package in R[90]. We
675 reported the marginal R^2 for each model, which describes the proportion of variance explained
676 by the fixed factors (not including random effects), implemented in the *MuMIn* package[91,92].
677
678 *Data availability*
679 DNA sequence alignments for the DIV p-loop of $Na_V1.4$ and the ddRADseq data will be
680 made available on GenBank upon manuscript acceptance. All phenotypic data and the code for
681 statistical analyses will be submitted to Dryad upon acceptance.
682

683 **Extended Data**
684
685 **Extended Fig. 1.** Functional analysis of phenotypic matching in populations of prey and
686 predator. The functional relationship of average adult *Ta. granulosa* total skin TTX (mg, log
687 scale) is plotted against the oral dose of TTX (mg, log scale) required to reduce the speed of an
688 average adult *Th. sirtalis* to 50% of baseline speed post-ingestion of TTX for each locality.
689 Individual points are colorized by the average level of newt TTX as in Fig. 1. Vertical bars
690 represent the full range of newt TTX values observed for each population; horizontal bars
691 represent the 95% confidence interval for the oral 50% dose of the corresponding snake
692 population. The dashed 50% line represents a functional match between newt TTX and snake
693 resistance: the dose of TTX in a newt that would reduce a snake of a given resistance to 50% of
694 its performance. The solid 15% and 85% lines (calculated as best-fit regressions for each
695 locality) delimit the range of functionally relevant TTX doses for snakes across the range of
696 sampled localities. Below the 85% line, values of TTX resistance are high enough for snakes to
697 consume co-occurring newts with no reduction in performance or fitness. Above the 15% line,
698 doses of newt TTX are so high that any snake that ingests a newt would be completely
699 incapacitated or killed. Localities with error bars that fall *entirely* outside the boundaries of these
700 lines (none of which were observed) are considered mismatched and regions where reciprocal
701 selection could not occur.
702

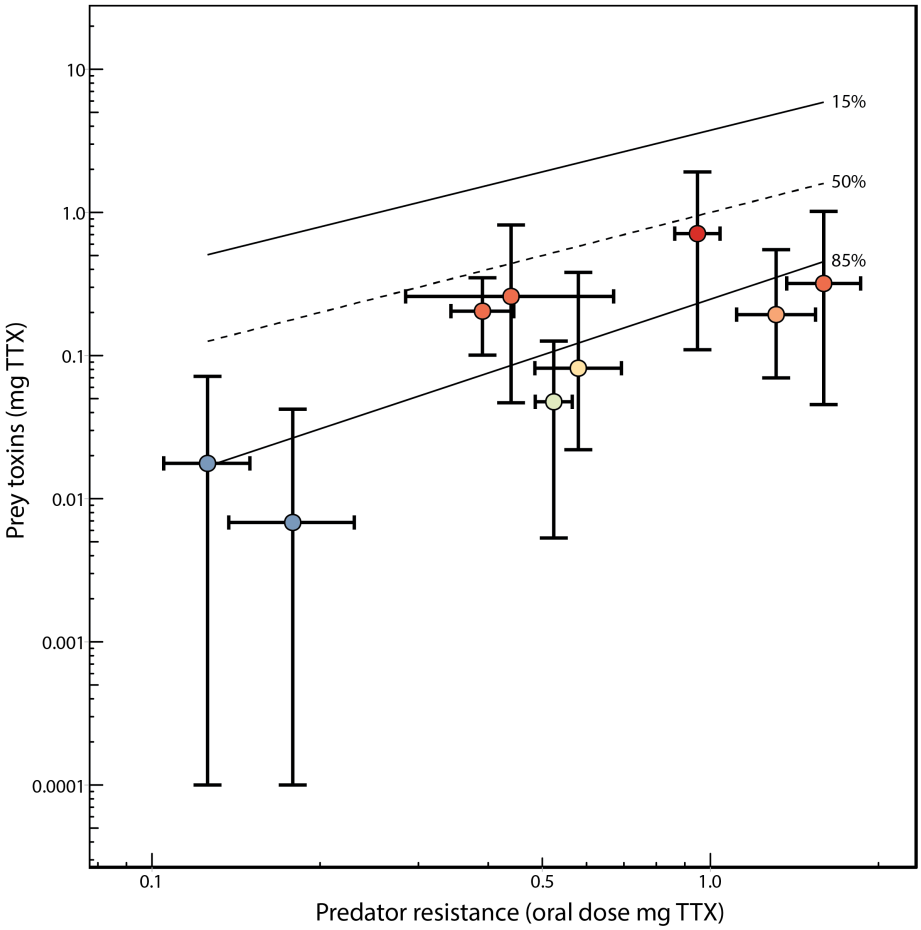

703
704

Extended Fig. 2. STRUCTURE results for K=2-4. The most likely number of genetic cluster was K=2 for both species (Fig. 2). STRUCTURE plots are arranged latitudinally by population, in the same order as the map. Each horizontal bar represents the ancestry assignment of an individual, with populations separated by white dashed lines.

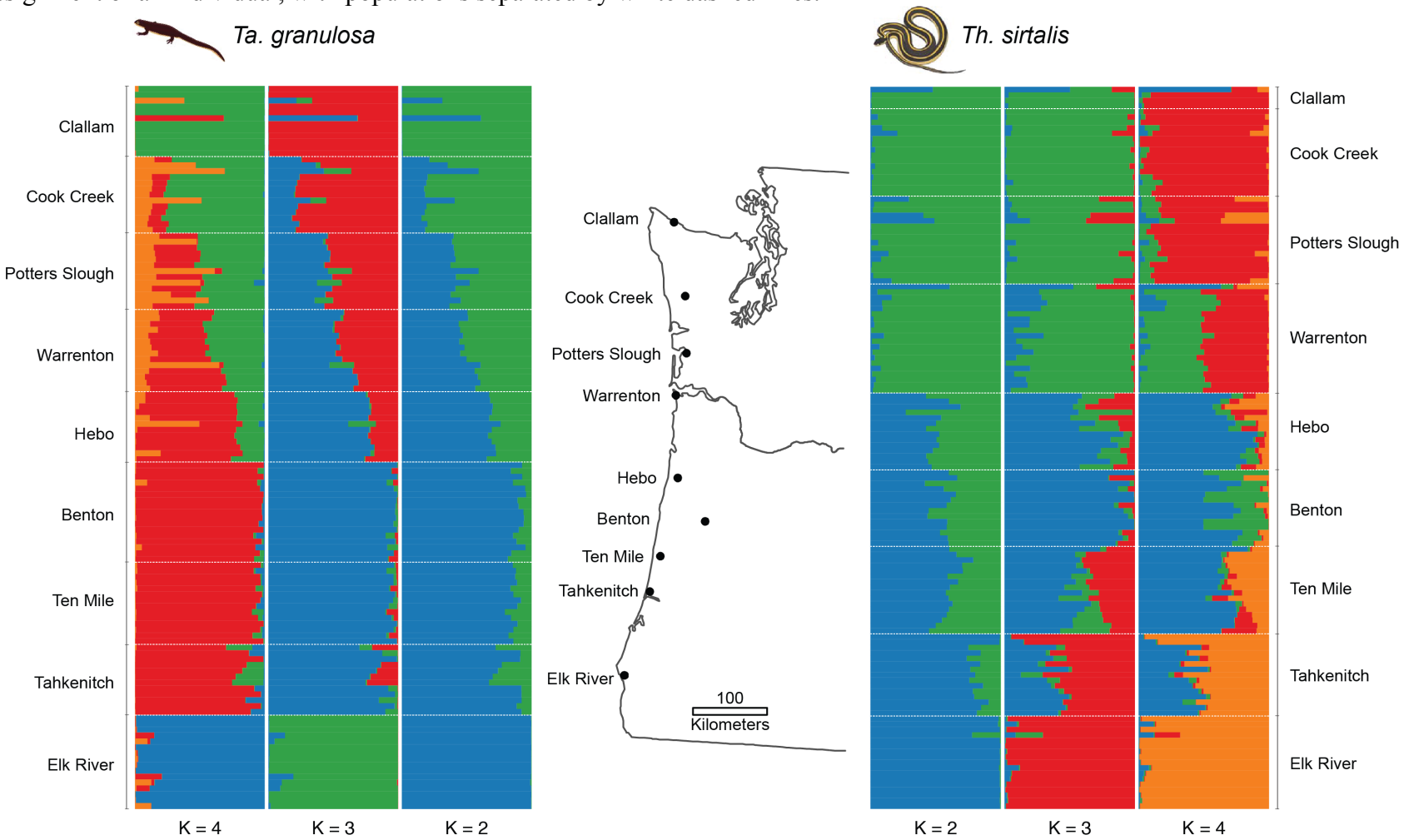
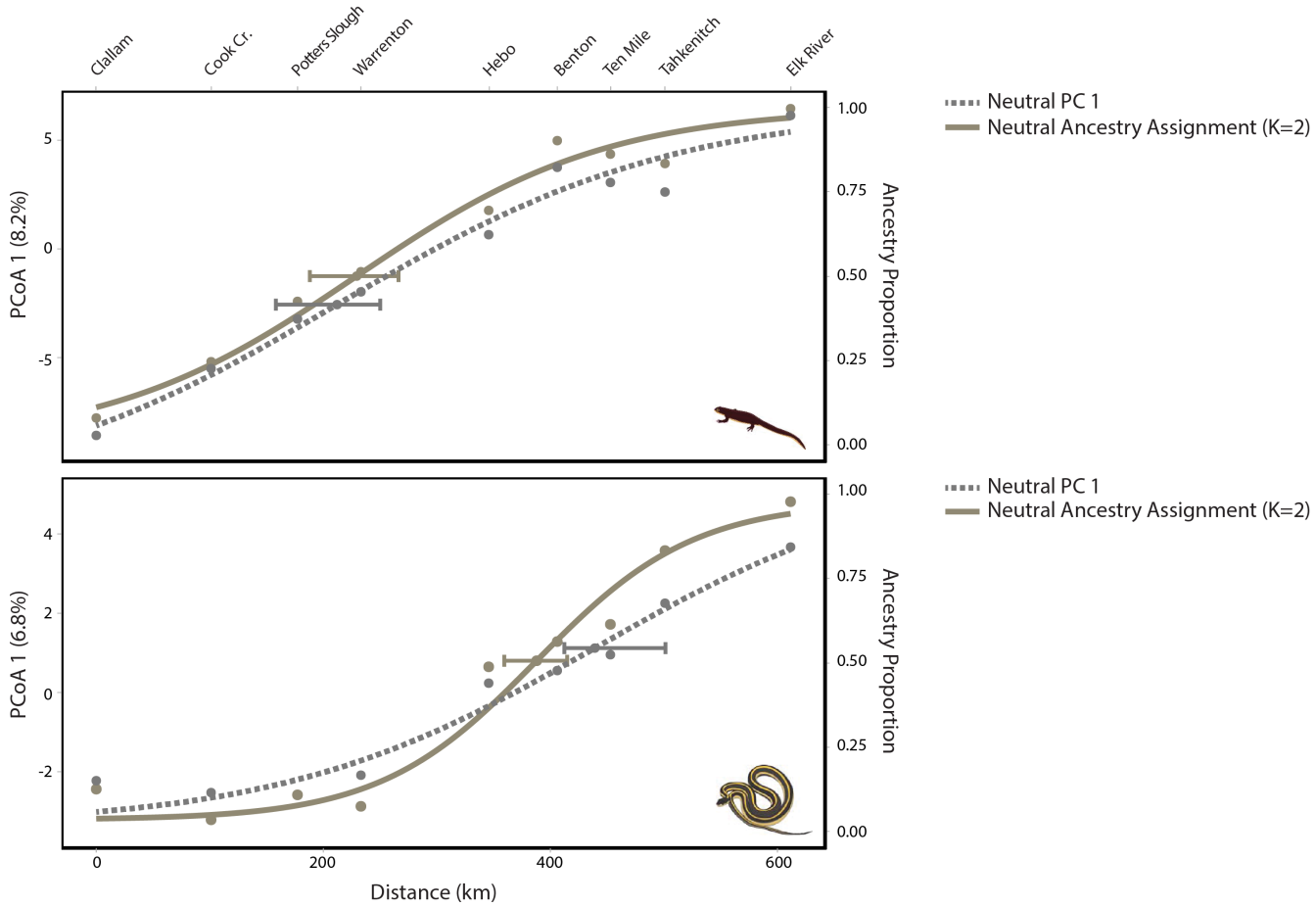
Extended Fig. 3. Comparison of neutral clines fit to (1) PC 1 values from the PCoA and (2) average ancestry assignment values (K=2) from the STRUCTURE analysis. Error bars indicate confidence intervals surrounding the geographic cline centers.